Mathematical Biosciences and Engineering

https://www.aimspress.com/journal/MBE

MBE, 21(4): 5762–5781.
DOI: 10.3934/mbe.2024254
Received: 16 January 2024
Revised: 08 March 2024
Accepted: 22 March 2024
Published: 25 April 2024

Research article

The switching and learning behavior of an octopus cell implemented on FPGA

Alexej Tschumak[1,*], **Frank Feldhoff**[2] **and Frank Klefenz**[3]

[1] Audio Communication Group, Technische Universität Berlin, Berlin, Germany
[2] Advanced Electromagnetics Group, Technische Universität Ilmenau, Ilmenau, Germany
[3] Fraunhofer Institute for Digital Media Technology, Ilmenau, Germany

[*] **Correspondence:** Email: tschumak@campus.tu-berlin.de.

Abstract: A dendrocentric backpropagation spike timing-dependent plasticity learning rule has been derived based on temporal logic for a single octopus neuron. It receives parallel spike trains and collectively adjusts its synaptic weights in the range [0,1] during training. After the training phase, it spikes in reaction to event signaling input patterns in sensory streams. The learning and switching behavior of the octopus cell has been implemented in field-programmable gate array (FPGA) hardware. The application in an FPGA is described and the proof of concept for its application in hardware that was obtained by feeding it with spike cochleagrams is given; also, it is verified by performing a comparison with the pre-computed standard software simulation results.

Keywords: dendrocentric backpropagation learning rule; synaptic subpopulation coactivation; collective synaptic weight adjustments; temporal logic

1. Introduction

Neuromorphic engineering models the basic collective processing of reservoir ensembles of spiking neurons. Recently, simple leaky integrate-and-fire neurons (LIF) have been enhanced with dendritic compartments [1]. The dendrocentric role is modeled by introducing populations of synaptic innervation sites that are spread across the dendrites, leading to relative dendritic delays from the synapses to the neuronal soma [2]. Sensory inputs are presented at the synaptic sites through the use of neurophysiologically based computational converter modules, which generate spike cochleagrams or visual input streams from the retina. The coactivation of synaptic subpopulations by orchestrated sensory input sequences enables proper event detection from the sensory streams.

We combined a computational auditory model, which served as a cochleagram generator with a computational dendritic model of an octopus cell. We modeled its sensory innervation and examined its switching and learning behavior according to sustained stimuli representations. Dendrocentric learning is achieved by selecting stimulus sequences according to the synapse subpopulations. Synaptic subpopulations are formed over time as a result of synaptic coactivation induced by a spike timing-depending plasticity (STDP) learning rule coordinated by a collectively timed backpropagation signal. The system is based on temporal logic that is applied in discrete time steps and replaces ion channel kinetics. The collective backpropagation STDP rule is directly implemented in field-programmable gate array (FPGA) hardware. The synapses have been modeled as ordinary weights in the range [0,1], converging in the steady state to either zero or one after the learning phase. The learning and switching behavior of the octopus cell has been modeled by using the hardware description language Verilog and realized on an FPGA development board.

Sensory processing is based on the conversion of sensory streams into categorical units such as pitch, color, and motion. The term pitch refers to frequency features present in a tonal signal like a sound, a melody, or the prosody of speech [3]. Multiple nuclei, consisting of ensembles of neurons of different cell types, work together to convert stimuli in the auditory pathway into the perception of pitch. A biologically inspired computational model of the auditory pathway is used to explain how the various neurons in the auditory nuclei interact and extract periodicity properties from auditory stimuli [4, 5]. The auditory pathway originates from the sensor inner hair cells, which stimulate connected spiral ganglion cells that bundle their axons to form the auditory nerve, which carries parallel spike trains to the auditory nuclei. The focus here is on the role of octopus cells in the posteroventral cochlear nucleus. Octopus cells connect via their dendrites, which span a highly branched tree, to innervating auditory nerve fibers (ANFs) in their receptive fields. Octopus cells arrange vertically along the tonotopic axis of the ANFs. The collective pitch processing scheme is determined by time which acts as a conductor in an orchestra. The role of octopus cells in this orchestra is elucidated in the time domain. Octopus cells encode periodicity by rhythmically firing in response to tonal signals. To analyze the pitch perception, the inter-spike intervals of consecutively firing octopus neurons are measured [6]. The distributions of inter-spike intervals of octopus cells form the basis for periodicity encoding [7].

Octopus cells adapt their firing behavior while they are permanently exposed to patterns in the event stream. They become accustomed to the presentation of repetitive stimuli and reduce their variability in neuronal impulse responses. In this way, they filter out the events that set the tone from the abundance of external stimuli in the environment. The octopus cell fires on specific triggers in the parallel ANF spike trains in its receptive field. The triggers are hyperbola-shaped delay trajectories in the spike cochleagrams. The octopus cell is able to decode them and rectify these hyperbolic trajectories through adaptive and repetitive learning of their temporal dynamics under the condition of the spatial synaptic arrangement along its shape-giving dendritic tree. It rectifies the delay trajectory by compensating relative ANF time delays by balancing dendritic path delays [8]. Depending on the involved synaptic contact sites and their spatial positions, unique situations arise in which input patterns match. All ANF spike-induced current potentials at the various synaptic sites converge at the soma. If they arrive at the soma at the same time, they can trigger an action potential and a backpropagation potential, which travels back into all dendritic branches. The backpropagation potential is the reinforcement signal. The backpropagating action potentials (bAP) lead to the formation of a collective subpopulation of coactive synapses. Those synaptic subpopulations are stabilized, coactive, and reinforced by many repetitive bAPs. Some synaptic subpopulations reach a steady state and reliably signal an event to occur because their synapses fired together many times.

Pre-sensitized synapses connect to a subpopulation by reinforcing their synaptic strengths via the backpropagation signal that passes through them. Learning is induced at synaptic sites when synapses are pre-sensitized by ANFs, and the backpropagation potential arrives at the pre-sensitized synapse within a certain time period before desensitization. In this case, the synaptic weights are collectively incremented. Multiple subpopulations can coexist and decode different patterns. A subpopulation triggers firing after a limited learning phase of about one hundred events of the same repetition type. The backpropagation learning rule represents classical STDP [9].

The octopus cell has been modeled as an LIF neuron with dendritc branches. The dendritic branches are represented as tentacles from the soma in the form of strands. Each tentacle is represented as a row in an array. Furthermore, each tentacle is represented as a separate delay chain consisting of a partition of uniform delay units. In the computational model, the travel time was calculated by taking the path length of the dendritic branch from synapse to soma divided by the assumed constant velocity. The delays were sampled at a clock frequency of 44.1 kHz, which is a standard sampling rate in audio codecs. The smallest differentiable delay unit was set as $\delta t = 22.67\,\mu\text{s}$. The delay chains were tuned in the microsecond range and were therefore able to detect acoustic signals. The spatial distribution of synapses was setup to control the dendritic computation by decoding the spatiotemporal synaptic input signals via temporal dynamics [10, 11].

Collective subpopulation learning on the hardware platform has been realized via the new backpropagation rule. Synaptic weights are stored and incremented or decremented in distributed memories in the FPGA [8]. Each synapse has been modeled as an ordinary weight variable [12,13]. FPGAs are programmable logic units. They have the advantage of being reconfigurable which makes them valuable for prototype development. Also, they can be tailored to execute a large amount of parallel operations. This allows for efficient computation and, hence, a small footprint. Based on the simulation results, we have reproduced the learning and switching behavior of an octopus cell in an FPGA.

2. Methods

2.1. *Pitch perception and auditory modeling*

Pitch as a perceptual category can be described as a periodic signal rather than a frequency [3]. Pitch perception is generated in the central auditory system [14, 15]. Although earlier models did autocorrelation studies with the focus solely on the output of auditory filters, newer models are being extended by developing physiological models that take auditory processing of the central nervous system into account [16].

The Fraunhofer IDMT stimulation-based auditory modeling (SAM) model used in this study converts fluctuating sound pressure levels into cochleagrams by simulating the biophysical processes that involve coupling the sound pressure fluctuations to tympani movements to induce vibrations of the ossicles. This triggers hydromechanical shock excitations of the fluid in the cochlea, which induces movements of the basilar membrane. This leads to deflection of the associated sensor inner hair cells, which triggers action potentials in the ANFs [4, 5]. A SAM-generated cochleagram for a sung vowel *a* is shown in Figure 1.

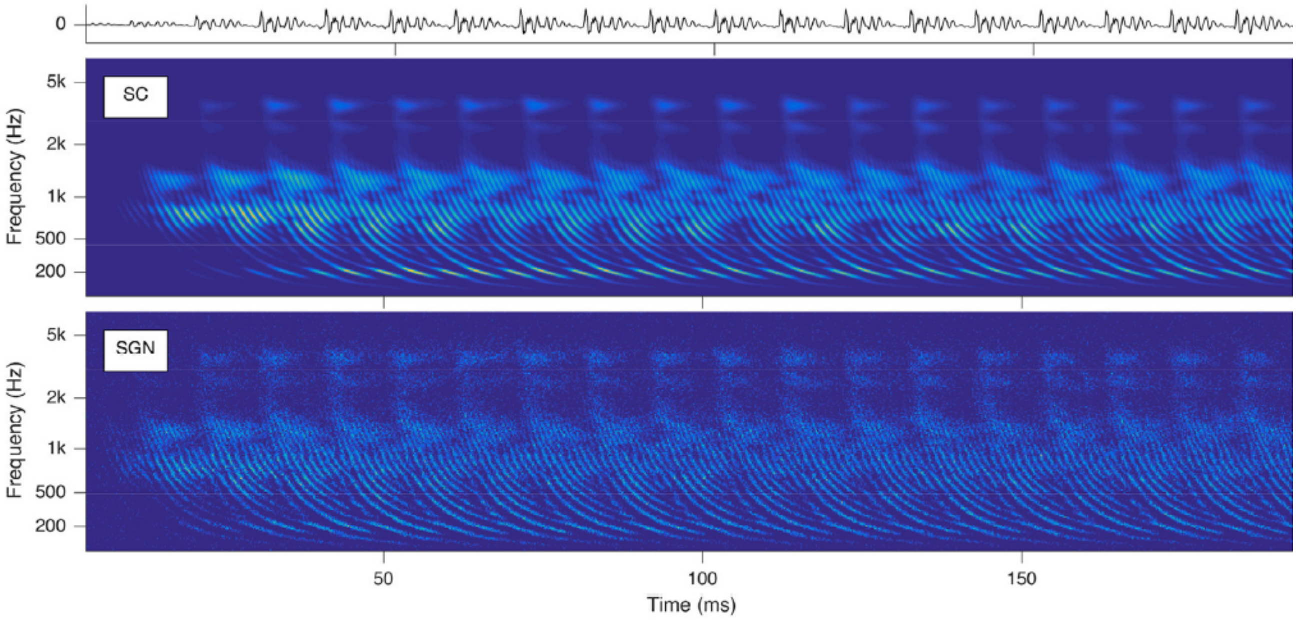

Figure 1. Cochleagrams with quasi-stationary repetitive patterns for a short snippet of the vowel *a* sung by a male singer at the note of G2. Top: Sound signal waveform. Middle: Probability (ascending from blue to green to yellow) of neurotransmitter substance release into the synaptic cleft (SC) as a function of time and place within the cochlea. Bottom: Action potentials of the spiral ganglion neurons (SGNs). Note that the ordinate shows the characteristic frequency of the basilar membrane model at the corresponding cochlear position. Reprinted with permission from [17].

Over time, octopus cell models have been developed and integrated into the SAM scheme by coupling them to ANFs. Octopus cells are sensitive to sections of ANF spike train trajectories in their receptive fields. Octopus cells fire rhythmically to sequential trajectories, and the inter-spikes are further processed by several nuclei in the auditory pathway to compute the inter-spike interval times. Various studies suggest that pitch estimation is based on interval distributions of the inter-spike trains of the octopus cells [18]. This assumption's advantage lies in its simplicity while being able to describe different kinds of pitch phenomena [19].

Based on this, a neurophysiological model which transforms inter-spike interval times into first spike latencies has been adapted for pitch perception and tested over two octaves for tones from the McGilles sample CD [17]. The results for C4–C6 are reprinted in Figure 2.

The neurophysiological form of the computational model is depicted in Figure 3. It consists of three layers, beginning with the octopus neuronal layer, which will be the sole focus of this work. Each octopus neuron fine-tunes itself to its local receptive field through the implementation of bAP-induced STDP when receiving ANF spike train inputs. One key aspect is that the synaptic learning occurs unsupervised. In the next step, formations of octopus cell outputs are processed in the subsequent inferior colliculus (IC) layer. It functions as a stopwatch that captures the intervals between the spikes (i.e., inter-spike intervals) that are coming from the octopus neuron's soma. Based on this, the pitch can be estimated in the pitch layer [6].

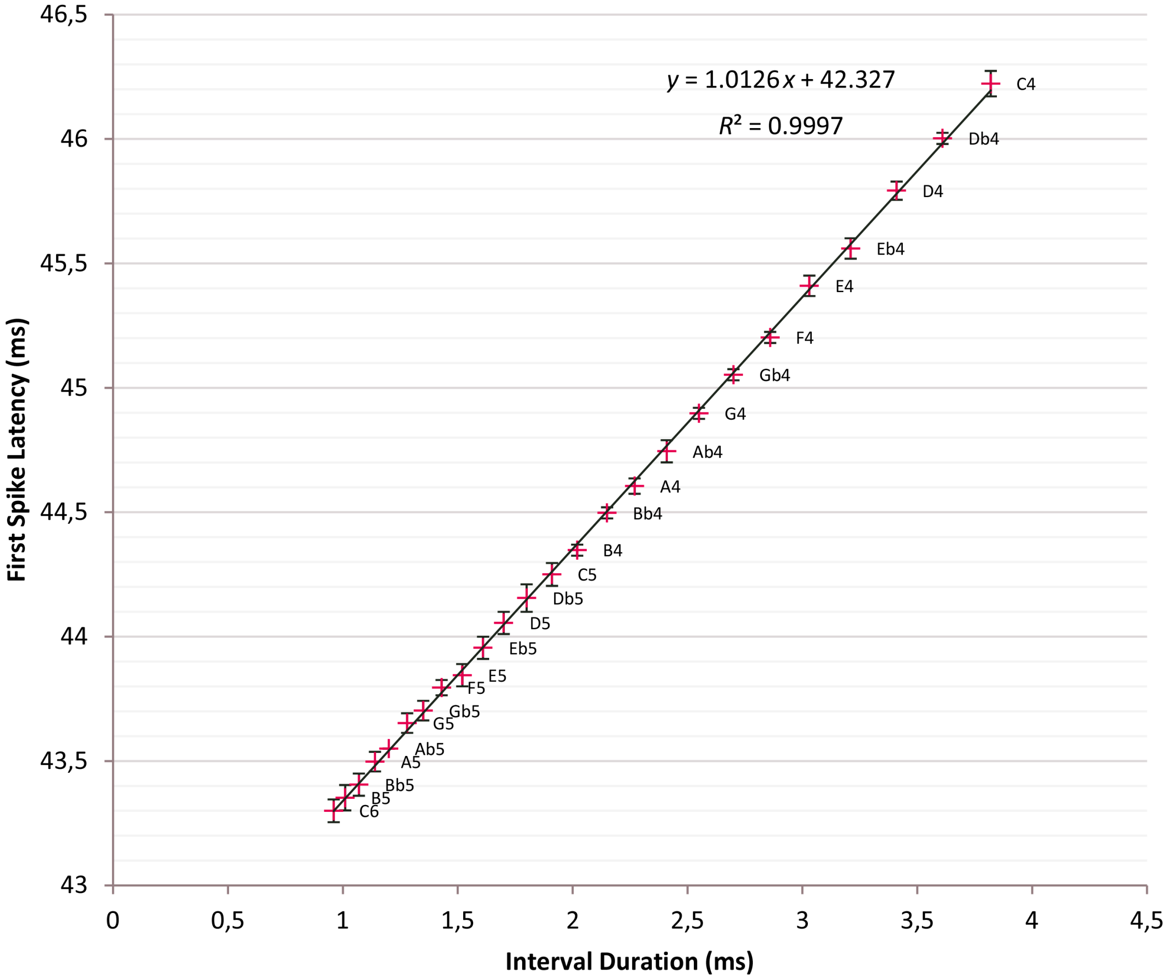

Figure 2. Time intervals versus first spike latencies (FSLs). Crosses: Tone intervals and corresponding FSLs; linear regression line fit: $y = 1.0126x + 42.327$, $R^2 = 0.9997$; error bars $\pm 2\sigma$; 95% confidence interval. Reprinted with permission from [17].

2.2. Dendritic computational models

Dendritic computational models [20,21] have been devised by using tools such as the neural analysis toolbox NEAT [22], or Dendrify, an open-source Python package based on Brian 2 [23]. Dendrify automatically generates reduced compartmental neuron models with simplified yet biologically relevant dendritic and synaptic integrative properties. Morphological neuron models have been created to model processes such as N-methyl-D-aspartate (NMDA) channels producing all or none localized dendritic responses, or dendritic Ca^{2+} spike mediation of the coincidence detection (CD) between distal inputs and somatic action potentials [24]. It has been found that sequence detection and direction selectivity may be more broadly applicaple methods of extracting temporal information than conventional mechanisms like CD [25].

Morphological models show that dendritic integration allows one to distinguish specific input patterns [26]. To model neurons with dendritic morphology on a neurophysiological level in NEURON is computationally costly [27]. Therefore, we chose to substitute the neurophysiological kinetics with

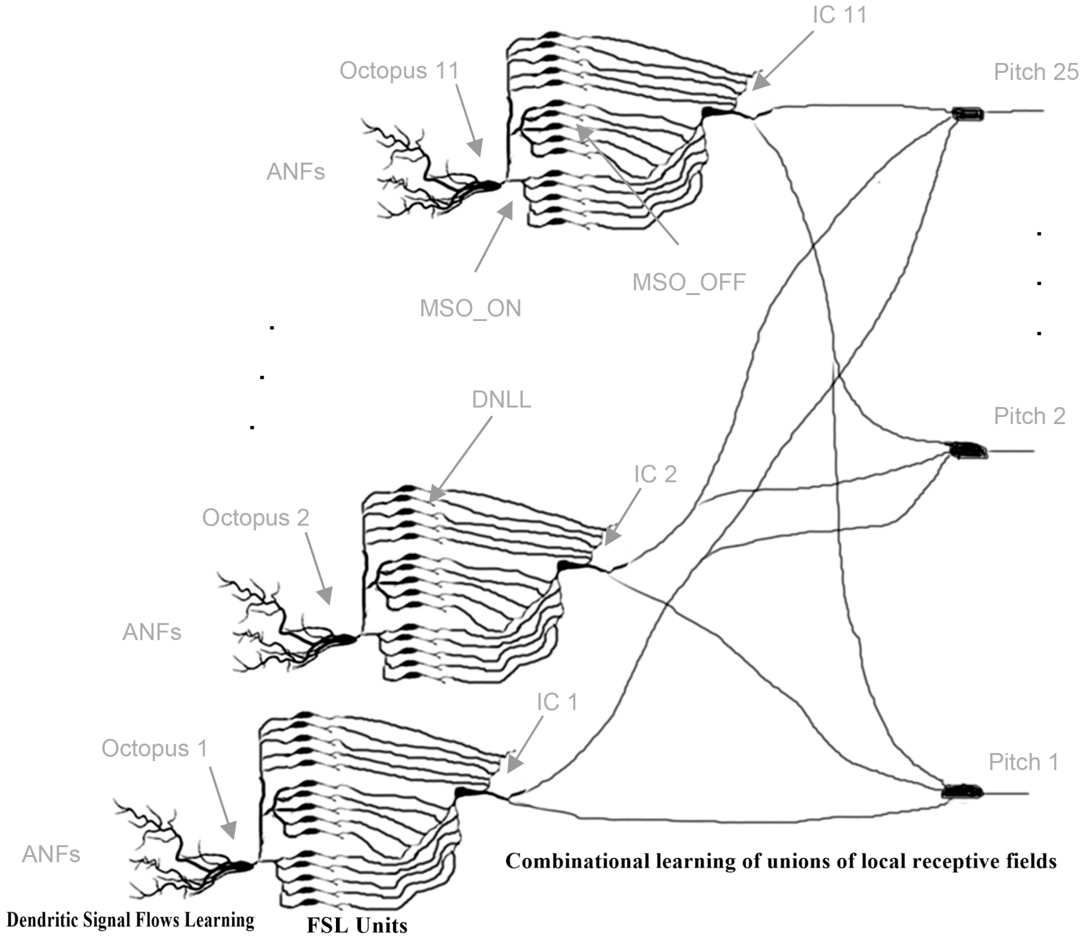

Figure 3. Three layers of periodicity pitch perception for cascaded learning: Starting from the left, octopus cells receive input from ANFs in their temporal receptive fields (three out of 11 are shown); Octopus cells trifurcate to MSO_ON neurons (i.e., bottom block: five out of 100 shown), MSO_OFF neurons (middle block: five out of 100 shown) and DNLL neurons (top block: five out of 200 shown); MSO_ON, MSO_OFF, and DNLL neurons connect to the bottom, middle, and top dendritic branches of the IC neurons; IC neurons connect to all pitch neurons (three out of 25 are shown). Reprinted with permission from [17].

temporal dynamics to equip our model with temporal logic operators as delays and synchronous coincidences in the time domain.

2.3. The new backpropagation learning rule

The existence and the mechanisms of bAPs initiated at the axonal site have been profoundly supported by the result of physiological studies [20]. The reported carriers involved in dendritic signaling include sodium ion channels, Ca^{2+} spikes, and NMDA spikes [28]. A single bAP generated at the axonal site serves as the post-reinforcement signal at the pre-sensitized synaptic sites in a pre-post time interval of about 4 ms. For example, calcium action potentials are initiated when they coincide with distal dendritic inputs within a time window of several milliseconds [29]. Our temporal model reproduces bAPs. Biological postsynaptic neurons have α-amino-3-hydroxy-5-methyl-4-isoxazolepropionic acid (AMPA) and NMDA receptors (AMPARs, NMDARs), which receive glutamates (one other type of neurotransmitters) to modulate cell excitability. NMDARs alone cannot activate the neuron's membrane potential. Activation requires correlated presynaptic and postsynaptic activities to upregulate the AMPAR insertions at the synaptic sites. Frequently activated synaptic connections are enhanced and unimportant connections are eliminated. We chose to model the synapse with NMDA and AMPA receptors, which need both pre- and postsynaptic activation conditions.

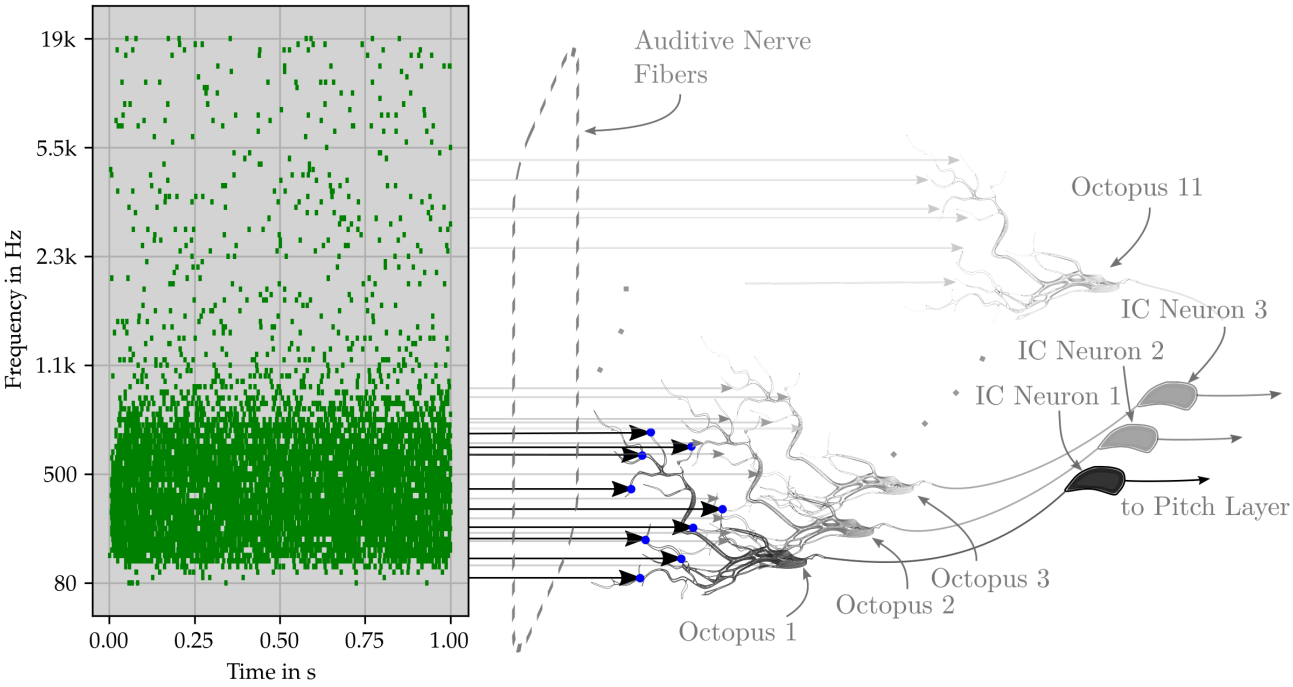

Figure 4. Illustration depicting the perceptual network. From the left to the right: An auditory model-generated ANF spike representation of a sound, which is then input into the octopus neuronal layer (four of 11 octopus neurons visible here). Each of them covers its own receptive field in the frequency range. The octopus axons project to the IC neurons (three of 11 IC neurons shown), which in turn connect to all pitch neurons. Reprinted with permission from [6].

The octopus model mimics the arbor morphology of the octopus cell. It is particularly designed to process spatiotemporal spike patterns through the application of temporal dynamics in its dendritic computation. Its dendritic tree encodes the spatiotemporal relationship of synaptic activation sites, the temporal flow dynamics and the backpropagation along all of the branches. We implemented the octopus cell with nine ANF connections in its receptive field. Therefore, it receives nine parallel temporal binned ANF streams [29]. We employed fixed time bins of $\delta t = 22.67\,\mu\text{s}$ because of the common audio sampling rate of 44.1 kHz. Each time bin codes a spike as logic 1 (0 otherwise). The ANF spikes are coded in the same way.

The theoretical background for the design of an octopus cell circuit was taken from a numerical model that provides a bio-plausible rule set to describe the behavior of octopus cells that are crucial for pitch discrimination methods. The realization of this numerical model can be seen in Figure 4. One objective of this study was to make it feasible for implementation on hardware [6].

2.4. *Octopus cell model layout*

The octopus cell is depicted as having a central body (soma) with branches (dendrites), and it is modeled by using specialized temporal logic operators [30, 31]. The system described in [6] relies on seven operators that form the set of stateful temporal logic operators that consist of min (FirstArrival), max (LastArrival), constant delay (D), inhibit (I), reset (R), coincidence (C), and memory (ON/OFF) [32]. There, inhibit (I) is unused, as it could be neglected without tradeoffs. Also, reset (R) is not needed because a synapse refractory time that sets the synapse to OFF after a preset time interval has triggered signal onset is sufficient [33]. The lengths of the dendritic pathways are measured in fixed time intervals represented by constant delays (D), with each interval set at δt = 22.67 µs. Memory storage occurs though the establishment of synaptic connections between ANFs and octopus dendrites. When a signal flows from its corresponding ANF, a synapse enters an active sensitized state, referred to as the ON state; otherwise, it remains in the OFF state. Min (FirstArrival) represents the first arrival of a signal from an ANF to the soma in its receptive field. Similarly, max (LastArrival) is the last incoming signal. The difference between the first arrival and last arrival is divided by the time step size and sets the number of steps and, therefore, the time window for occurring interactions in the system. Coincidence (C) is realized when currents gathered at the soma cross the set threshold value.

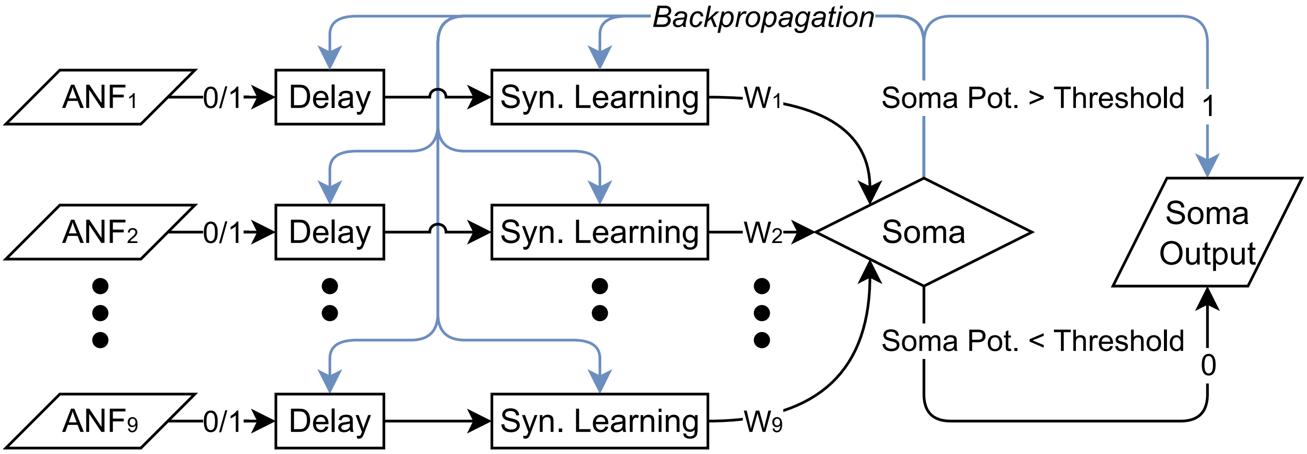

Figure 5. Signal flow in the octopus cell model. The two directions of the model can be seen here: The black arrows describe the forward propagation and light blue arrows indicate the backpropagation for the soma output module, the delay, and the synaptic learning modules. '0/1' at the ANF inputs and soma output underlines their 1-bit depth for the inputs and outputs of the model.

The dendrites create a directed acyclic graph, with the direction determined by the propagation state (whether forward or backward), guiding them toward either the soma or synaptic connections [6]. The organization of modules and signal flow of the octopus cell model on the FPGA is shown in Figure 5. For the forward propagation, each input is passed through its individual shift registers that delay incoming signals. Each shift register has a learning module attached that attenuates an incoming signal based on the current synaptic weight and passes it on to the soma module. There, incoming impulses are summed as the soma membrane potential until a threshold is crossed. As a result, a spike output signal is generated from the soma, and, simultaneously, backpropagation is initiated. BAP signals are transmitted from the soma module back to the other modules to terminate the processing of incoming signals and enable synaptic learning. Once the bAP has reached the farthest dendritic path, forward propagation resumes.

2.4.1. Forward propagation

The model starts with the forward propagation, where $A_{\mathrm{i,j}}(t)$ is the input matrix with i as the index representing the ANF channel and j is the time index for the corresponding time t. Each input is passed through its own shift registers that delay (D_i) incoming signals. These delays represent the path, that is, from the ANF along the dendritic branches to the soma that each impulse has to traverse. The delays of each pathway are determined by the Greenwood function that is commonly used for cochlear implants to determine the frequency in the organ of Corti [34]:

$$f = 165.4 \cdot \left(10^{2.1 \cdot x} - 0.88\right) \mathrm{Hz}. \tag{1}$$

Variable x represents the relative position on the cochlea, with it equal to one at the apex of the basilar membrane and zero at the opposite end. The reciprocal core frequency f returns the period which will be discretized by the sample unit time. The resulting delay values used in this model can be seen in Figure 6.

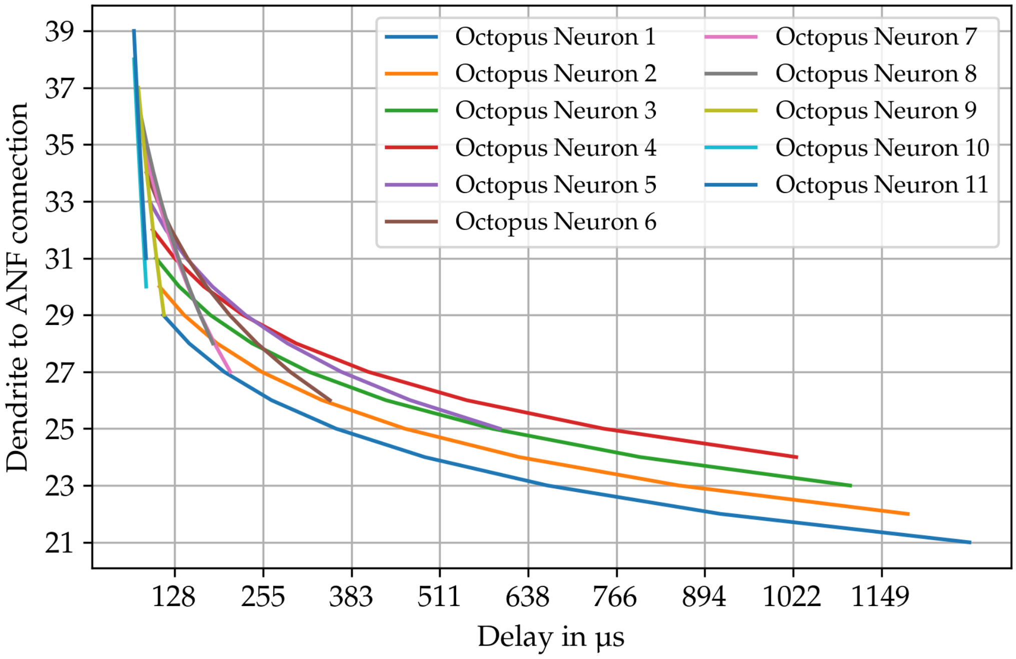

Figure 6. Dendritic delays have been calculated according to Eq (1). The specific delay is shown on the x axis and the connected auditory nerve fiber on the y axis. The templates for the delay curves are superimposed as in the actual model. Taken with permission from [6].

After the impulses propagate through the shift register modules, each delayed impulse coming from ANF channels adds a value to the adder module (representing the soma) determined by the current synaptic weight $W_{\mathrm{i,j}}(t)$ of the learning module. A refractory phase for each synapse arriving at the learning module is also included. This is realized by applying a counter variable that counts down the predefined refractory time steps when a signal arrives at the learning module. This ensures that the synapse is active for the duration of the refractory phase. When there was no input signal within the refractory phase, the synapse will be deactivated.

All incoming values to the adder module are summed to be the soma membrane potential $Soma_{\mathrm{j}}(t)$, as dependent on t:

$$Soma_{\mathrm{j}}(t) = Soma_{\mathrm{j}}(t_{\mathrm{prev}}) - dc + \sum_{i=1}^{n} A_{\mathrm{i,j}}(t - D_{\mathrm{i}}) \cdot W_{\mathrm{i,j}}(t). \tag{2}$$

Here, n is the total number of ANF channels within one neuron. A constant decay, dc, for the soma membrane potential to represent soma leakage. When the soma membrane potential crosses the predefined threshold represented by the variable $thresh$, the function of the adder module can be described as follows:

$$\begin{aligned}
&\text{If } Soma_{\mathrm{j}}(t) - thresh > 0 : \\
&\qquad Spike_{\mathrm{j}}(t) = 1, \\
&\qquad bAP_{\mathrm{j}}(t) = 1, \\
&\qquad Soma_{\mathrm{j}}(t) = 0; \\
&\text{else} : \\
&\qquad Spike_{\mathrm{j}}(t) = 0, \\
&\qquad bAP_{\mathrm{j}}(t) = 0;
\end{aligned} \tag{3}$$

This leads to a soma stimulus response that initiates a spike output $Spike_{\mathrm{j}}(t)$ of the neuron. Simultaneously, a backpropagation signal is initiated and the soma depolarizes to its resting state (i.e., soma membrane potential value is reset to zero).

2.4.2. Backpropagation and synaptic learning

When the backpropagation is activated, a backpropagating action potential is sent to all shift registers and synaptic learning modules. This signal leads to all shift registers ignoring incoming values from the ANF inputs because of a change to a correspondingly sized, zero-filled array while the backpropagation is active. Furthermore, this will lead to zero output signals in the synaptic learning modules.

The synaptic learning scheme adheres to the STDP rule. A synapse is activated by glutamatergic vesicles from the presynaptic ANF, entering an active state (pre-conditioning). The soma-triggered action potential initiates backpropagation (post-conditioning) into dendrites. For synaptic weight adjustment, the synapse must be active and sensitized, with backpropagation activation before desensitization. Synapses contain both AMPA and NMDA channels. AMPARs start at zero, with their max conductance matching that of NMDARs. Active synaptic weights, $W_{\mathrm{i,j}}(t)$, change during somatic backpropagating action potential triggers [6]:

$$W_{\mathrm{i,j}}(t)_{\mathrm{update}} = W_{\mathrm{i,j}}(t) + (Lr \cdot Syn_{\mathrm{i}} \cdot bAP_{\mathrm{j}}(t)). \tag{4}$$

Table 1. Synapse update parameters.

Variable	Value
Syn_{i}	0/1
$bAP_{\mathrm{j}}(t)$ signal	0/1
Learning rate (Lr)	0.01

In the learning module, for each synapse that was active in the previous forward propagation cycle (Syn_{i} → 'ON'), a $bAP_{\mathrm{j}}(t)$ signal (→ 'ON') will increase the synaptic weight according to the learning rate Lr (i.e., assertion of the STDP learning rule). For example, if the maximum synaptic weight is set to one and the AMPAR value starts at zero, it would take 100 backpropagation cycles at a learning rate of 0.01 to reach max conductance. The backpropagation is active until the distance of the longest dendritic pathway in the neuron has been traversed by the bAP signal. This will be realized by taking the time step size of the longest shift register in the perceptive field to be initialized as a counter that counts down when the backpropagation starts. As soon as the countdown becomes zero, forward propagation for all modules is activated again. Now, the shift register modules receive ANF inputs again. And, in the learning modules, Syn_{i} is set to 'OFF'.

2.5. *Simulation and implementation on an FPGA*

The development started with a behavioral simulation of the model by replicating one octopus neuron. Subsequently, the model was adjusted to facilitate implementation on a PYNQ-Z2 Advanced Kit FPGA board (ZYNQ XC7Z020-1CLG400C). This board was equipped with a multiprocessor system-on-chip design that can implement a processing system and programmable logic on one device. The implementation was then executed on the FPGA board with the objective of verifying that it produces deterministic results that are consistent with the behavioral simulation. Following successful verification of one octopus neuron, the model was expanded to run all octopus neurons in parallel, allowing for experimentation with different sets of parameters.

2.5.1. Behavioral simulation

The process of configuring, designing, simulating, and testing the circuit involved the utilization of Vivado 2022.1. Vivado is a software development environment and integrated development environment created by AMD-Xilinx. For the simulation, all modules that form one octopus neuron, as shown in Figure 5, were configured by using the hardware description language Verilog. The use of floating-point values has been avoided and the model was scaled up to have integers (i.e., corresponding learning rate from 0.01 to 10, threshold from 4.5 to 4500). Using floating-point values in FPGAs can be less efficient, as floating-point arithmetic typically requires significantly more resources than fixed-point or integer arithmetic. The bit depth of the entire system depends on the precision that needs to be reproduced. For example, to be able to use lower soma decay values, the bit depth of the soma membrane potential needs to be increased.

2.5.2. Implementation setup

After conducting a behavioral simulation on the Vivado platform and achvieving the anticipated results, further design work for the implementation was carried out by using Vivado's IP integrator. A wrapper called the "octopus module" was created; it instantiates and connects all modules mentioned in the prior simulation step. It also serves as an interface for all incoming and outgoing signals. The setup of modules can be seen in Figure 7.

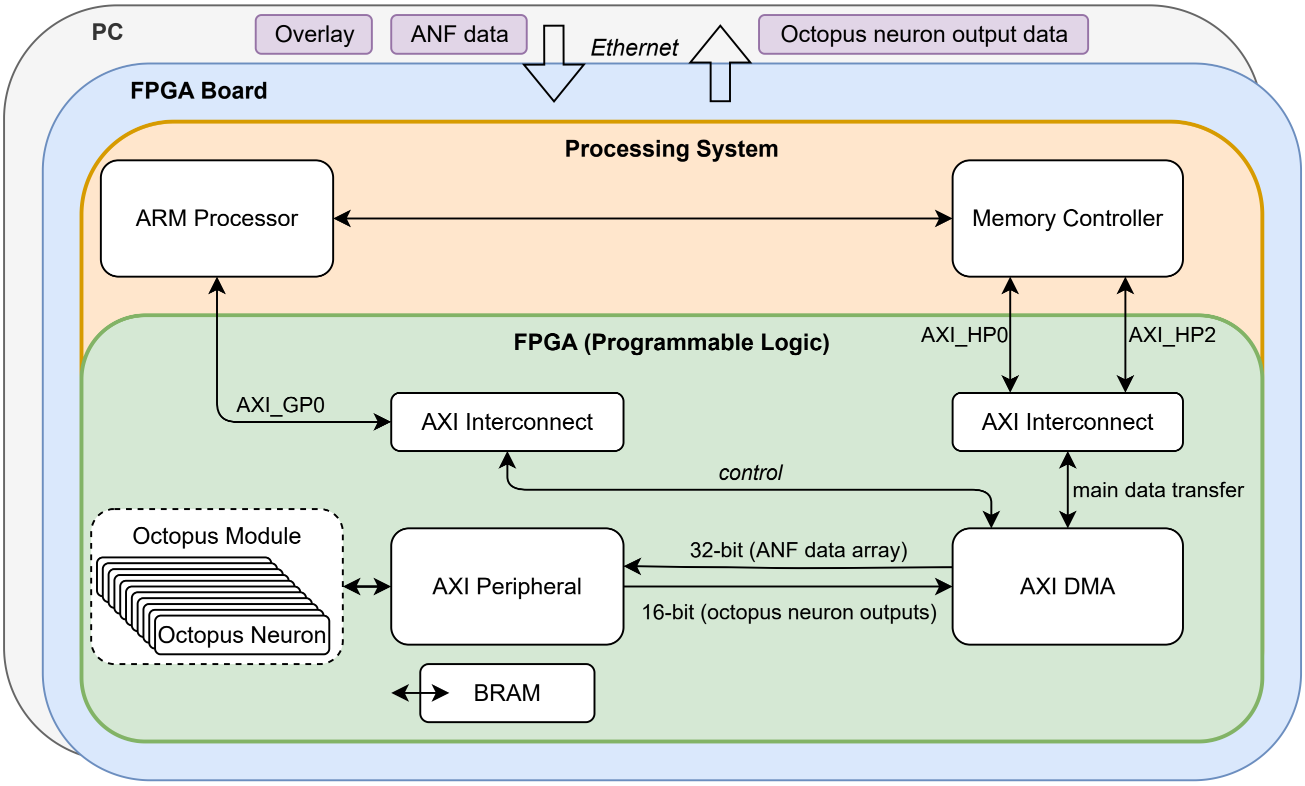

Figure 7. The FPGA implementation utilizes IP cores for the processing system, DMA, AXI interconnects, an AXI peripheral, and the octopus wrapper module. The connection between a PC and the FPGA board was established via Ethernet. The PC hosts the PYNQ software framework on the FPGA board. The overlay and ANF data are transferred to the FPGA board, which sends out the system's octopus neuron output data. Regarding data transfer between the memory controller and the DMA, two high-performance ports ('AXI_HP0' and 'AXI_HP2') were utilized. A general-purpose AXI port ('AXI_GP0') initiates the start of operation in the DMA.

Xilinx's own intellectual property (IP) modules, namely, the ZYNQ7 Processing System, Advanced eXtensible Interface (AXI) Peripheral, and AXI Direct Memory Access (AXI DMA), have been added to the design. Vivado's IP integrator automatically added the Processor System Reset IP module and three AXI Interconnect IP modules. The AXI is a standard interface protocol that is widely used in digital design and embedded systems to facilitate communication between various hardware components, including microprocessors, memory controllers, and peripherals. The AXI DMA module allows for communication between the programmable logic and the system memory. The AXI Peripheral IP was customized to suit the octopus module's inputs and outputs and enable data transmission. Apart from this adjustment, default configurations of the ZYNQ7 Processing System IP, AXI interconnects, and the AXI DMA were used. To imitate a stream of data, the whole array of ANF input data was first loaded into the system memory at once. Particularly, on the AXI slave (receiving from the DMA) side, the whole ANF spike train array is iterated during runtime into the octopus module input ports when a 't_ready' and a 't_valid' signal comes from the AXI master (sending to the DMA) side.

This results in high usage of the block RAM (BRAM), which was limited to 630 kB on the FPGA board and reserved for high-performance tasks. Simultaneously, the octopus module output is written into the system memory on the AXI master side during runtime. The previously mentioned step size of $\delta t = 22.67$ µs, which was derived from the 44.1 kHz sampling rate, indicates that the FPGA system is running at a significantly higher frequency (i.e., the default processing system's clock speed was 100 MHz).

2.5.3. Running the octopus cell model on an FPGA

Following the completion of the simulation and synthesis procedures for the design, an overlay was generated within the Vivado environment. Overlays are flexible hardware designs that can be loaded onto an FPGA without reconfiguring the entire FPGA, allowing for the switching of configurations. To execute the overlay, the PYNQ software framework (version 3.0.1) was employed. In the Jupyter notebook, an overlay class and a DMA class were instantiated. In the notebook, ANF input data were then sent through the DMA to the input buffers. The AXI DMA itself was connected to the AXI streaming ports. The model's output data were retrieved from the DMA class's output buffer in the Jupyter notebook.

3. Results

To test the model by using the aforementioned software and hardware, a sample from the already mentioned SAM auditory model was used as input data [4]. It yielded bio-plausible ANF spike trains (Figure 8) that were derived from a cochleagram of a sine tone in C4 (261.63 Hz). The data had a 44.1 kHz sampling rate, with 101 8-bit channels (one channel per ANF) and a duration of one second. Each ANF channel represents a bandpass frequency spanning 85 to 19,078 Hz.

The parameters in Table 2 were used to run the simulation and implementation on the FPGA.

The learning rate was selected to require 50 backpropagation cycles for a synapse to achieve a maximum conductance value of one. The resource utilization for the FPGA system can be seen in Table 3. In this model, all ANF input data were loaded onto the FPGA system at once, which explains the relatively high percentage of BRAM usage. This is worth mentioning, as the intended application environment was designed to have a continuous stream of data input and output rather than a static array. Smaller data packages would result in accordingly smaller BRAM allocations.

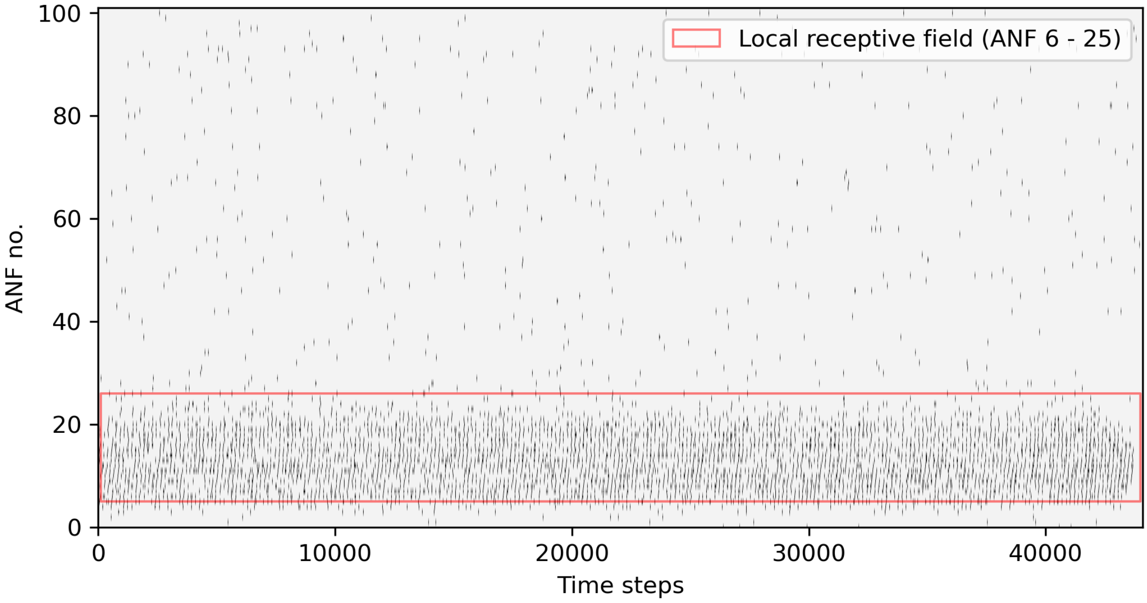

Figure 8. ANF spike trains provided by the SAM model for a sine C4. The local receptive field is contained in the red box. This range of ANF inputs was used as direct input for the model.

Table 2. Configuration parameters.

Parameter	Value
Soma threshold	3000
Learning rate	0.01
Synapse refractory time	2 ms
Soma decay	15
NMDA initial value	500
Timescale	22.67 µs

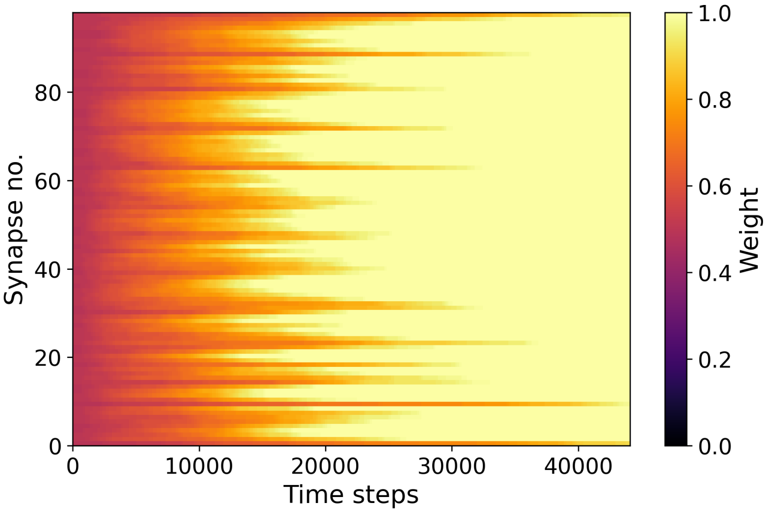

Figure 9. Evolution of synaptic weights over time.

Table 3. Resource utilization on a PYNQ-Z2 Advanced Kit FPGA board.

Resource	Available	Util. of one neuron (%)	Util. of all neurons (%)
Lookup Tables (LUT)	53,200	5.2	12.3
LUT-Based RAMs (LUTRAM)	17,400	1.3	1.9
Flip-Flops (FF)	106,400	4.4	7.6
Block RAM (BRAM)	140	85	85
Clock Buffers (BUFG)	32	3.1	3.1

The simulation of the octopus neuron output was found to be identical to the hardware FPGA output. Figure 9 illustrates the progressive upregulation of the synaptic weights of all ANF-octopus synapses for the receptive field of octopus neurons 1–11. In Figure 10, the inter-spike interval distributions of all neurons are depicted as boxplots.

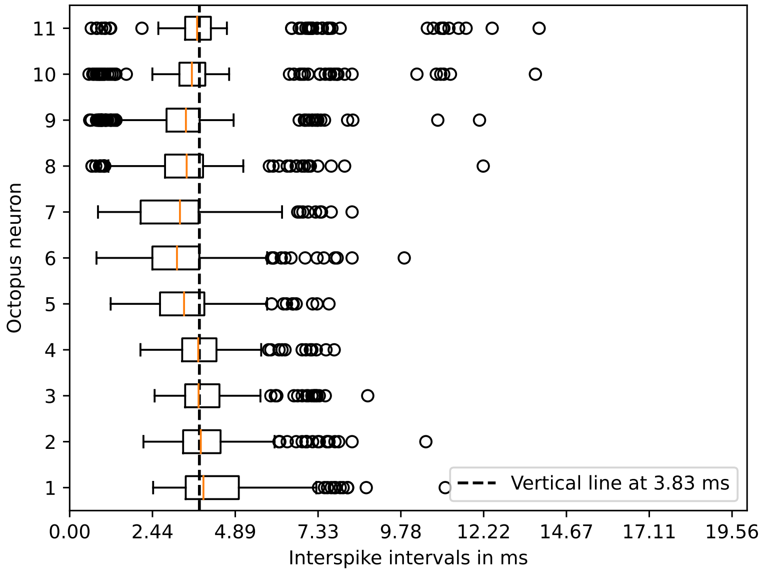

Figure 10. Inter-spike intervals of neurons 1–11 for a sine signal in C4. The period of the sample is shown as a vertical line.

In addition, 8-bit channels were determined to yield an adequate word length for extraction of the synaptic weight values (i.e., to accommodate the maximum value of synaptic weight of 100). Also, one 16-bit channel was built in to retrieve the data on the soma membrane potential. These channels were implemented for testing purposes and are not needed for the basic functionality. Regarding the latter, only a 1-bit channel is necessary for the soma output signal.

4. Discussion

The functionality of the octopus cell model, as well as its results was found to be consistent between the simulation and hardware implementation. The core aspects of collective online learning and switching behavior of the octopus neuron model on an FPGA have been demonstrated. Considering that neuronal networks and, hence, neuromorphic computing, require an increasing number of resources, optimized hardware systems can significantly improve performance for complex dendritic tasks [35].

The simplicity of the model, which directly translates into its feasibility and scalability, is evident in the small amount of resources required to execute the model on the FPGA. Neglecting BRAM utilization, it becomes feasible to concurrently operate the full set of 11 octopus neurons, effectively encompassing the frequency spectrum of the local receptive field. This would provide the first layer for periodicity pitch perception, as in [6]. Regarding the BRAM allocation, it could be significantly reduced by reducing the allocation size for the AXI inputs and outputs. Because the core part of the model has been written in the Verilog hardware description language, it can be adapted to other FPGA architectures. Future research could focus on a hardware implementation for the subsequent IC and pitch layers. Furthermore, the next step could involve integrating the octopus cell model into a real-time auditory streaming environment, such as research to simulate it in conjunction with neuromorphic auditory sensors [36]. The hardware model can be integrated into artificial intelligence systems and combined with self-adaptive population mechanisms, or convolutional long short-term memory networks or gated recurrent unit models [37, 38].

Another possible field of application could be the use of FPGAs that operate on a nanostructural level and replicate brain-like signal processing for robotics or sensory processing that would be able to work under harsh conditions [39]. Furthermore, since this work only utilized ANF spike train data from a sine tone, future work could involve fine-tuning this model's parameters to suit a variety of different sample materials. One limiting factor could be that, when there are smaller delay compensations, the model is limited by the time-bin structure derived from the sampling rate. This could be overcome by higher sampling rates of the cochleagram input. The choice of parameters such as delay compensations or decay was found to have a significant effect on the performance. Because configuring and testing the FPGA can be a longer processes than that required for the software, it is recommended first to fine-tune the optimal set of parameters in the behavioral simulation. Also, the amount of values one can extract to investigate the performance of the design is restricted by the technical capabilities of the FPGA (for example, the streaming bandwidth). This again implies that experimenting with different sets of configurations should be carried out at the simulation level.

5. Conclusions

We have proposed a reconfigurable solution path for collective online learning of the octopus cell and demonstrated its switching behavior showing its temporal dynamics to be well-matched to its sensory signals of interest. Also, we have proposed an algorithm–circuits co-design approach and validated it by conducting circuit simulations and running it on an FPGA development board, demonstrating the proper operation of the learning rule and the correct switching behavior. The concept has been proven through the use of a single bio-plausible sample. To this end, future research could investigate the performance of the model for a broad variety of samples or the hardware implementation of the subsequent layers of cascaded learning in periodicity pitch perception. Lastly, future work will include interfacing the FPGA with an event-based streaming converter that has been supplied by continuous auditory streams.

Use of AI tools declaration

The authors declare that they have not used artificial intelligence tools in the creation of this article.

Acknowledgments

FK, FF, and AT developed the ideas and composed the main part of the manuscript. AT programmed the hardware model, conducted the proof of concept in the FPGA, and created the plots. During the drafting process, all three contributed to the discussions, revisions, and proofreading of the manuscript. All authors contributed to the article and approved the submitted version. All authors agree to be accountable for the content of the work.

We acknowledge the support from the German Research Foundation and the Open Access Publication Fund of TU Berlin. This work was partially supported by Carl Zeiss Stiftung within the framework of the project Memwerk and the project Quantum Hub Thuringia, grant number 2021 FGI 0048.

Conflict of interest

The authors declare that there is no conflict of interest.

References

1. B. A. Bicknell, M. Häusser, A synaptic learning rule for exploiting nonlinear dendritic computation, *Neuron*, **109** (2021), 4001–4017. https://doi.org/10.1016/j.neuron.2021.09.044
2. K. Boahen, Dendrocentric learning for synthetic intelligence, *Nature*, **612** (2022), 43–50. https://doi.org/10.1038/s41586-022-05340-6
3. D. J. Hermes, *Pitch Perception*, Springer International Publishing, Cham, (2023), 381–448. https://doi.org/10.1007/978-3-031-25566-3_8
4. T. Harczos, A. Chilian, P. Husar, Making use of auditory models for better mimicking of normal hearing processes with cochlear implants: The sam coding strategy, *IEEE Trans. Biomed. Circuits Syst.*, **7** (2013), 414–425. https://doi.org/10.1109/TBCAS.2012.2219530
5. T. Harczos, *Cochlear Implant Electrode Stimulation Strategy Based on a Human Auditory Model*, PhD thesis, Ilmenau University of Technology, 2015.
6. F. Feldhoff, H. Toepfer, T. Harczos, F. Klefenz, Periodicity pitch perception part III: sensibility and pachinko volatility, *Front. Neurosci.*, **16** (2022), 736642. https://doi.org/10.3389/fnins.2022.736642
7. M. A. Rutherford, H. von Gersdorff, J. D. Goutman, Encoding sound in the cochlea: from receptor potential to afferent discharge, *J. Physiol.*, **599** (2021), 2527–2557. https://doi.org/10.1113/JP279189
8. M. Cartiglia, A. Rubino, S. Narayanan, C. Frenkel, G. Haessig, G. Indiveri, et al., Stochastic dendrites enable online learning in mixed-signal neuromorphic processing systems, in *2022 IEEE International Symposium on Circuits and Systems (ISCAS)*, IEEE, (2022), 476–480. https://doi.org/10.1109/iscas48785.2022.9937833

9. M. Saponati, M. Vinck, Sequence anticipation and spike-timing-dependent plasticity emerge from a predictive learning rule, *Nat. Commun.*, **14** (2023), 4985. https://doi.org/10.1038/s41467-023-40651-w

10. H. Zheng, Z. Zheng, R. Hu, B. Xiao, Y. Wu, F. Yu, et al., Temporal dendritic heterogeneity incorporated with spiking neural networks for learning multi-timescale dynamics, *Nat. Commun.*, **15** (2024), 277. https://doi.org/10.1038/s41467-023-44614-z

11. V. Francioni, M. T. Harnett, Rethinking single neuron electrical compartmentalization: dendritic contributions to network computation *in vivo*, *Neuroscience*, **489** (2022), 185–199. https://doi.org/10.1016/j.neuroscience.2021.05.038

12. M. Payvand, F. Moro, K. Nomura, T. Dalgaty, E. Vianello, Y. Nishi, et al., Self-organization of an inhomogeneous memristive hardware for sequence learning, *Nat. Commun.*, **13** (2022), 5793. https://doi.org/10.1038/s41467-022-33476-6

13. M. Payvand, S. D'Agostino, F. Moro, Y. Demirag, G. Indiveri, E. Vianello, Dendritic computation through exploiting resistive memory as both delays and weights, in *Proceedings of the 2023 International Conference on Neuromorphic Systems*, ICONS '23, Association for Computing Machinery, New York, NY, USA, (2023), 1–4. https://doi.org/10.1145/3589737.3605977

14. A. J. M. Houtsma, J. L. Goldstein, The central origin of the pitch of complex tones: Evidence from musical interval recognition, *J. Acoust. Soc. Am.*, **51** (2005), 520–529. https://doi.org/10.1121/1.1912873

15. Y. H. Li, P. X. Joris, Case reopened: A temporal basis for harmonic pitch templates in the early auditory system, *J. Acoust. Soc. Am.*, **154** (2023), 3986–4003. https://doi.org/10.1121/10.0023969

16. L. Faye, S. Kuhn, A. Venkatesh, Relative periodicity of empirical audio samples with application to dissonance perception, *LASER J.*, **1** (2023), 6.

17. F. Klefenz, T. Harczos, Periodicity pitch perception, *Front. Neurosci.*, **14** (2020), 486, https://doi.org/10.3389/fnins.2020.00486

18. G. D. Langner, *The Neural Code of Pitch and Harmony*, Cambridge University Press, 2015.

19. R. Meddis, L. O'Mard, A unitary model of pitch perception, *J. Acoust. Soc. Am.*, **102** (1997), 1811–1820. https://doi.org/10.1121/1.420088

20. Y. Yang, X. Li, H. Li, C. Zhang, Y. Todo, H. Yang, Yet another effective dendritic neuron model based on the activity of excitation and inhibition, *Mathematics*, **11** (2023), 1701. https://doi.org/10.3390/math11071701

21. M. Sinha, R. Narayanan, Active dendrites and local field potentials: Biophysical mechanisms and computational explorations, *Neuroscience*, **489** (2022), 111–142. https://doi.org/10.1016/j.neuroscience.2021.08.035

22. W. A. Wybo, J. Jordan, B. Ellenberger, U. Marti Mengual, T. Nevian, W. Senn, Data-driven reduction of dendritic morphologies with preserved dendro-somatic responses, *Elife*, **10** (2021), e60936. https://doi.org/10.7554/eLife.60936

23. M. Pagkalos, S. Chavlis, P. Poirazi, Introducing the dendrify framework for incorporating dendrites to spiking neural networks, *Nat. Commun.*, **14** (2023), 131. https://doi.org/10.1038/s41467-022-35747-8

24. E. Baek, S. Song, Z. Rong, L. Shi, C. V. Cannistraci, Neuromorphic dendritic computation with silent synapses for visual motion perception, Preprint, 2023. https://doi.org/10.20944/preprints202306.0438.v1

25. H. W. Lu, P. H. Smith, P. X. Joris, Mammalian octopus cells are direction selective to frequency sweeps by excitatory synaptic sequence detection, *Proc. Natl. Acad. Sci.*, **119** (2022), e2203748119. https://doi.org/10.1073/pnas.2203748119

26. R. Makarov, M. Pagkalos, P. Poirazi, Dendrites and efficiency: Optimizing performance and resource utilization, *Curr. Opin. Neurobiol.*, **83** (2023), 102812. https://doi.org/10.1016/j.conb.2023.102812

27. J. Kaiser, S. Billaudelle, E. Müller, C. Tetzlaff, J. Schemmel, S. Schmitt, Emulating dendritic computing paradigms on analog neuromorphic hardware, *Neuroscience*, **489** (2022), 290–300. https://doi.org/10.1016/j.neuroscience.2021.08.013

28. M. E. Larkum, J. Wu, S. A. Duverdin, A. Gidon, The guide to dendritic spikes of the mammalian cortex *in vitro* and *in vivo*, *Neuroscience*, **489** (2022), 15–33. https://doi.org/10.1016/j.neuroscience.2022.02.009

29. L. Benatti, T. Zanotti, D. Gandolfi, J. Mapelli, F. M. Puglisi, Biologically plausible information propagation in a complementary metal-oxide semiconductor integrate-and-fire artificial neuron circuit with memristive synapses, *Nano Futures*, **7** (2023), 025003. https://dx.doi.org/10.1088/2399-1984/accf53

30. A. Madhavan, M. Stiles, Storing and retrieving wavefronts with resistive temporal memory, in *Proceedings of the IEEE International Symposium on Circuits and Systems*, Seville, (2020), 1–5. https://doi.org/10.1109/ISCAS45731.2020.9180662

31. A. Madhavan, M. W. Daniels, M. D. Stiles, Temporal state machines: Using temporal memory to stitch time-based graph computations, *J. Emerg. Technol. Comput. Syst.*, **17** (2021), 1–27. https://doi.org/10.1145/3451214

32. G. Tzimpragos, D. Vasudevan, N. Tsiskaridze, G. Michelogiannakis, A. Madhavan, J. Volk, et al., A computational temporal logic for superconducting accelerators, in *Proceedings of the Twenty-Fifth International Conference on Architectural Support for Programming Languages and Operating Systems*, (2020), 435–448. https://doi.org/10.1145/3373376.3378517

33. J. E. Smith, Space-time algebra: A model for neocortical computation, in *Proceedings of the 45th Annual International Symposium on Computer Architecture*, ISCA '18, IEEE Press, (2018), 289–300. https://doi.org/10.1109/ISCA.2018.00033

34. D. D. Greenwood, A cochlear frequency-position function for several species—29 years later, *J. Acoust. Soc. Am.*, **87** (1990), 2592–2605. https://doi.org/10.1121/1.399052

35. T. Li, J. Tang, J. Chen, X. Li, H. Zhao, Y. Xi, et al., Monolithic 3d integration of dendritic neural network with memristive synapse, dendrite and soma on Si CMOS, in *2023 China Semiconductor Technology International Conference (CSTIC)*, (2023), 1–3. https://doi.org/10.1109/CSTIC58779.2023.10219334

36. D. Gutierrez-Galan, A. Rios-Navarro, J. P. Dominguez-Morales, L. Duran-Lopez, G. Jimenez-Moreno, A. Jimenez-Fernandez, Interfacing PDM MEMS microphones with PFM spiking systems: Application for neuromorphic auditory sensors, *Neural Process. Lett.*, **55** (2023), 1281–1292. https://doi.org/10.1007/s11063-022-10936-0

37. P. Cai, Y. Zhang, T. Jin, Y. Todo, S. Gao, Self-adaptive forensic-based investigation algorithm with dynamic population for solving constraint optimization problems, *Int. J. Comput. Intell. Syst.*, **17** (2024), 1–17. https://doi.org/10.1007/s44196-023-00396-2

38. Z. Yao, Z. Wang, D. Wang, J. Wu, L. Chen, An ensemble cnn-lstm and gru adaptive weighting model based improved sparrow search algorithm for predicting runoff using historical meteorological and runoff data as input, *J. Hydrol.*, **625** (2023), 129977. https://doi.org/10.1016/j.jhydrol.2023.129977

39. T. Tsuchiya, T. Nakayama, K. Ariga, Nanoarchitectonics intelligence with atomic switch and neuromorphic network system, *Appl. Phys. Express*, **15** (2022), 100101. https://doi.org/10.35848/1882-0786/ac926b